ることを確認している[12]．また，これを相転移温度以上に再加熱して徐冷しても hcp 構造には変わらないことから，超急冷プロセスによる非平衡状態としての高温相が生成されたのではなく，全自由エネルギーの観点からこの微粒子サイズでの安定状態として fcc 構造をとることを指摘している．筆者らは Fe 微粒子について，TEA CO_2 レーザーを使用した気相化学反応により，これまで単離することができなかった高温 (910～1390℃) 安定相の γ-Fe 微粒子を室温で高選択的に高収率で生成している[13]．すなわち，Fe $(CO)_5$ と SF_6 との混合物に TEA CO_2 レーザー光を平行光で照射すると，SF_6 赤外光増感作用によって $Fe(CO)_5$ が分解し，最終生成物として γ-Fe 微粒子を生成することができる．この方法で室温安定相である α 相を γ 相に対して数%程度に抑え，90%以上の選択性で γ-Fe を生成できる．γ-Fe は面心立方構造をとっており，バルク体では，個々の Fe 原子は 12 個の最近接配位の Fe 原子をもつことになるが，粒子表面では結合手の破断によりそれ以下の配位数となる．その局所的な対称性の欠如を結晶電場勾配（四重極相互作用）の形としてメスバウアースペクトルはとらえている[9]．ちなみにこの γ-Fe 微粒子の磁性であるが，1.8 K の温度まで下げても磁気秩序状態は現れず常磁性であることを観測している[14]．

イオン性物質での粒子表面の対称性欠如の影響は，大きな単位胞サイズを通して内部まで及ぶこととなり，バルク体とは異なるイオン配置や空格子の出現，温度によるイオンの再配列など，エネルギー的にわずかでも有利なさまざまな形の特異構造を誘発しバルク体とは異なる固有の物性を呈することとなる．イオン性微粒子の生成でも構造相転移や異相混合等の介在で格子歪は導入され，後述のように磁気特性に影響を与えることとなる．

5. 固有磁化における特異性

微粒子の固有磁化にまつわる特異性はイオン性物質での観測例が多い．いくつかの例を提示して，特異な磁性とその起因について概説する．前出の core-shell model と non-collinear magnetic structure の顕在については，既報のいくつかのレビュー[1),7),8)]を参照されたい．

5.1 Mn-ferrite の磁気転移温度（ネール点）の粒子サイズ依存

立方晶系スピネル型フェライトの 1 単位胞は 8 化学式からなり，1 化学式は (A)[B_2]O_4 で示されるので 24 個の金属イオンと 32 個の酸素イオンで構成されている (Fig. 1)．金属イオンは 4 個の酸素イオンに囲まれた四面体位置 (A) と，6 個の酸素イオンに囲まれた八面体位置 (B) の 2 種類の副格子からなっている．

Mn-ferrite ($MnFe_2O_4$) の場合を考える．バルク体でのイオン配置は中性子線回折やメスバウアー分光より，$(Mn_{0.8}Fe_{0.2})[Mn_{0.2}Fe_{1.8}]O_4$ で与えられている．液相反応法

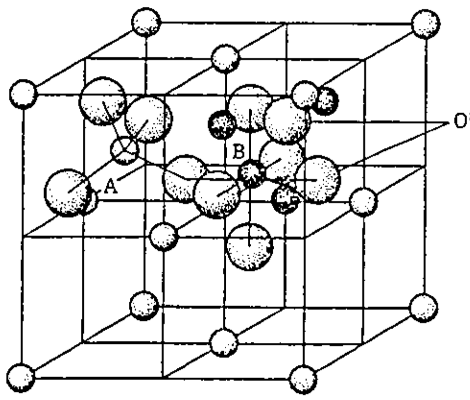

Fig. 1 One unit cell of a spinel lattice. All the ion positions are shown for two octants only. The symmetries at the tetrahedral (A) and octahedral (B) sites are indicated.

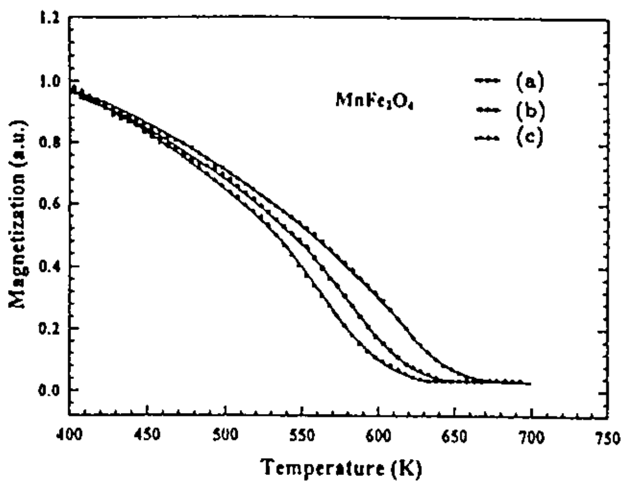

Fig. 2 Magnetization of Mn-ferrite spherical particles with average diameters of (a) 15, (b) 21, and (c) 30 nm.

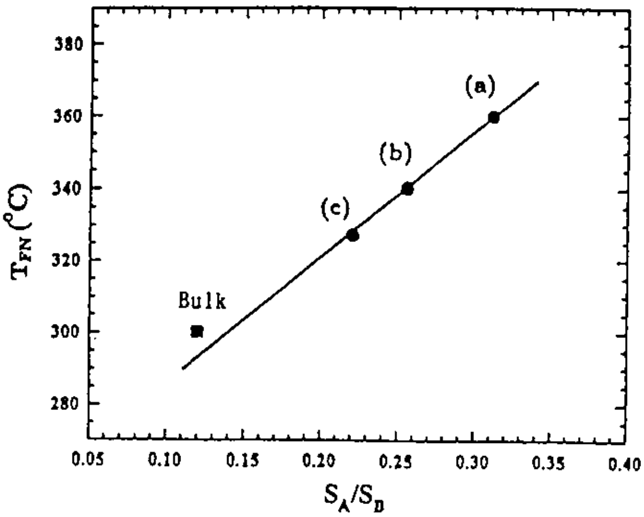

Fig. 3 Ferromagnetic Néel temperature (T_{FN}) of Mn-ferrite particles and the value for the bulk material *vs.* S_A/S_B. S_A and S_B are the relative iron occupancies of the A and B sites as determined from in-field Mössbauer spectra.

で生成した$MnFe_2O_4$微粒子(16, 21, 30 nm)について，Mnイオンの原子価変動に配慮した速やかな昇温速度で熱磁化曲線(Fig. 2)よりネール温度の測定をしたところ，その結果はFig. 3に示すようにバルク体の573 Kより高く，粒子サイズが小さいほど高い傾向（それぞれ637, 612, 600 K）にあることが判明した[15]．その原因について，6Tの高磁場下でのFe^{57}のメスバウアースペクトル測定を調べたところ，Feイオン配置が粒子サイズで異なっていることが明らかとなった（A副格子スペクトルが粒子サイズの縮小に伴い増加）[16]．フェライト系物質では，Fe (A)–Fe (B) 交換相互作用が強磁性の支配的要因であることを考えるとFig. 3は理解できる結果である．イオン配置が粒子サイズで異なり，磁気特性に変調を引き起こしている一例である．加えて高磁場下でのメスバウアースペクトル結果は，この物質もご多分にもれず6 Tの磁場でも配向しないnon-collinearの磁気構造が存在することを示しており，筆者らが，かつて提唱したcore-shellモデルの普遍性を示す結果である．

5.2 Zn-ferrite（常磁性物質）の強磁性的振舞

バルク体のZnフェライト($ZnFe_2O_4$)では，Znイオン（非磁性）が選択的にA位置を占める結果，イオン配置は$(Zn)[Fe_2O_4]$となり，B位置のFeイオンがこの物質の磁性を律することとなる．この物質の磁性は約10 K付近にネール温度があり，それ以下の温度ではB–B間の相互作用のために反強磁性となるが，この温度以上ではその相互作用は非常に弱く常磁性になるとされている．したがって通常の固相反応で得られるZn-ferriteは磁石にほとんど付かない．しかし液相反応で得た超微粒子の場合はなぜか磁化をもち，77 Kでは強く磁石に付くようになる[17]．多結晶質のZn-ferriteを高速ボールミルで粉砕して得た微粒子でも同様である[15]．筆者らの中性子線回折実験や高磁場下メスバウアー分光の結果より，微粒子Zn-ferriteにおいては小量のFeイオンがA位置を占め，その量は微粒子化とともに増すことが判明した[18]．すなわち微粒子状態ではA-site空間とB-site空間とで，Znイオンが選択的にA-site空間に入るほどの自由エネルギー差がなくなっており，微粒子化につれてB-site空間をも占めるようになる．その結果FeイオンがA-site空間に入る量が増すこととなる．すると強いA–B間の相互作用が磁気クラスター的な形で芽生えることとなる．これが外部磁場に応答することになる．通常サイズのZn-ferriteでも，わずかな量の置換は常に起こっているようで，これにまつわる多くの研究がなされている．

5.3 Yttrium-iron-garnet (YIG) の特異磁性と構造

YIG ($Y_3Fe_5O_{12}$)の1単位胞は8化学式からなり，そのイオン配置は1化学式あたり2個のFeイオンが八面体位置[a]，3個のFeイオンが四面体位置(d)，3個のYイオンが十二面体位置c-siteを占めており$Y_3[Fe_5]O_{12}$で表記される．

液相反応・焼成によって生成したYIG微粒子に付き，4.2 Kおよび300 Kでの飽和磁化値σ_sを比表面積(S.S.A.)に対してプロットすると，いずれもほぼ一直線にのって比表面積の増加（微粒子化）につれ減少する[19]．微粒子の磁性に表面構造が関与していることを如実に物語っている．同様の傾向は，non-collinearな磁気構造を示すフェライト系やCrO_2などのイオン性（絶縁性）強磁性体で広く一般的に観測されている[2),10)]．粒子表面層の特異磁性が関係しており，この直線の勾配よりYIG粒子の表面層1.8 nm厚は飽和磁化に寄与していない（磁場方向に配列しない）とすると理解できる結果である．また，S.S.A.=0（大きな粒子の比表面積に対応）へのσ_sの外挿値は，4.2 Kおよび300 Kともに低く，固相反応など通常のYIGバルク値のおよそ60%である．高磁場下でのメスバウアー分光からは，spin canting構造の存在に加えて，[a], (d)両副格子のFeイオンの存在比はバルク体と同じ2:3であることが得られており，液相反応YIGには[a], (d)両副格子のFeイオン位置にそれぞれ同程度の相当量の空格子があって，Feイオンの磁化への寄与が減少していると考えると理解できる[19]．

また，YIG微粒子における金属イオンのmisplacementは特徴的である．生成法によっては小量のFeイオンはc-siteにも入りうる(Fe anti-site defect)し，また小量のYイオンは比較的に大きな空間のa-siteにも入りうる(Y anti-site defect)ことが，Fe^{57}のNMRの測定で明らかにされている[20)~22)]．

Fig. 4は，YIG微粒子の4.2 Kでの固有保磁力を比表面積に対してプロットしたものである[23]．保磁力にも粒子表面層の関与があることを示唆する結果である．粒子サイズが極端に小さな領域で直線性から外れているのは熱的ゆら

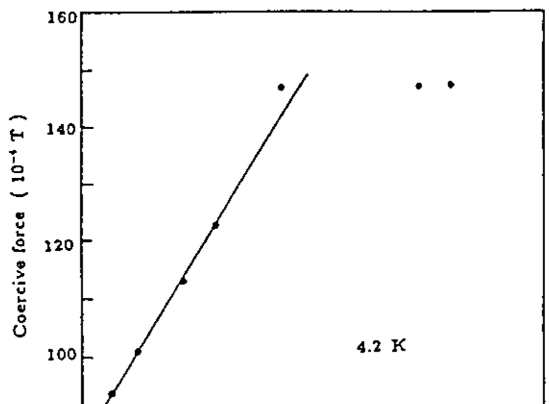

Fig. 4 Coercive force of YIG particles with various surface areas at 4.2 K.

ぎによるものと思われる．

6. 格子歪によるフェライト系微粒子の磁気的硬質化

微粒子の magnetic hardening のメカニズムは，これまで結晶磁気異方性や形状磁気異方性に起因するものが大部分である．表面磁気異方性や歪磁気異方性が付与された形でさらなる磁気的硬質化も考えられる．

6.1 表面磁気異方性の顕在

諸々の磁性微粒子に対する phenomenological anisotropy constant は，超常磁性にまつわる磁化の緩和時間の測定などから得られている．一般に当該物質のバルク値で観測されている値に比べてすこぶる高く，何らかの付加的な異方性の重畳が示唆される．例えば γ-Fe_2O_3 の結晶磁気異方性定数 $[K_1]$ は 4.6×10^3 J/m^3 のバルク値に対し，粒子サイズ 6 nm での観測値は 1.2×10^5 J/m^3 にもなる[24]．表面磁気異方性を最初に言及したのは Néel である[25]．表面の結晶対称性の変化による結晶磁気異方性の変化からもその由来は容易に推察できる．Néel は結晶磁気異方性を近隣する原子対間の相互作用の和としてとらえ，現象論的なアプローチを行っている．表面磁気異方性の値は小さいが，10 nm 以下の大きさの粒子にとっては重要であると結論している．その後，金属薄膜などで多くの実験がされており，例えば Fe や Co 薄膜ではある厚さ以下の膜では磁化が膜面に垂直に配向することが報告されている[26]．

6.2 歪磁気異方性導入による磁気的硬質化

ある種のフェライト粒子においては，熱処理に伴う粒子内の構造変化で歪が導入され，歪磁気異方性に起因の硬質化した磁気特性が期待できる．例えば，Cu フェライト ($CuFe_2O_4$) 粒子は 360℃以上の温度領域から徐冷されることにより立方晶から正方晶へ構造相転移を起こす．八面体位置を占める Cu イオンによる Jahn–Teller 効果がその原因とされている．現実にこれによる磁気的硬質化が観測されている[27]．また Mn フェライト ($MnFe_2O_4$) 粒子においては熱処理条件に伴う Mn イオンの原子価変動（酸化・還元）により，空格子の生成・消滅が粒子内に起こる．これらによる構造変化に伴い粒子内に歪が導入され，歪磁気異方性に起因の硬質磁気特性が期待できる．さらに単一磁区粒子の超微粒子構造が加われば，磁化過程の上でいっそうの硬質化が見込まれる．これらの発想に基づき $Mn_{1.7}Fe_{1.3}O_4$ 粒子で 4000 Oe の保磁力が報告されている[28]．

マグネタイト (Fe_3O_4) は人類が遭遇した最初の天然磁石である．この Fe_3O_4 微粒子は大気中で徐酸化するとガンマ酸化鉄 (γ-Fe_2O_3) 微粒子となる．この徐酸化の過程で保磁力が増大し，ある酸化領域で極大値をとることはよく知られている[29]．微粒子薄膜ではよりいっそう顕著な増加が観測されている[30]．Fe_3O_4 と γ-Fe_2O_3 は構造が似て非なるところがある．いずれもスピネル型ではあるが前者は立方晶系，後者は厳密には正方晶系であり，格子定数の違いのほかに γ-Fe_2O_3 には構造的な空格子がありしかも秩序配列している．これが超格子構造として回折実験で観測される．しかし微粒子状態では，空格子の秩序配列がくずれており構造面からの識別は難しい[31]．異相混合状態で磁気的硬質化が得られているのは事実であり，混合相に起因の格子歪が何らかで関与していると思われる．

Table 1 Values of the material parameters used in calculations

Material parameters	Value
Saturation magnetization (Ms [A/m])	1700E3
Exchange stiffness (A [J/m])	21E-12
Crystalline anisotropy (K1 [J/m^3])	48E3
Surface anisotropy constant (edge K1 [J/m^3])	Variable
Anisotropy type:	Uniaxial

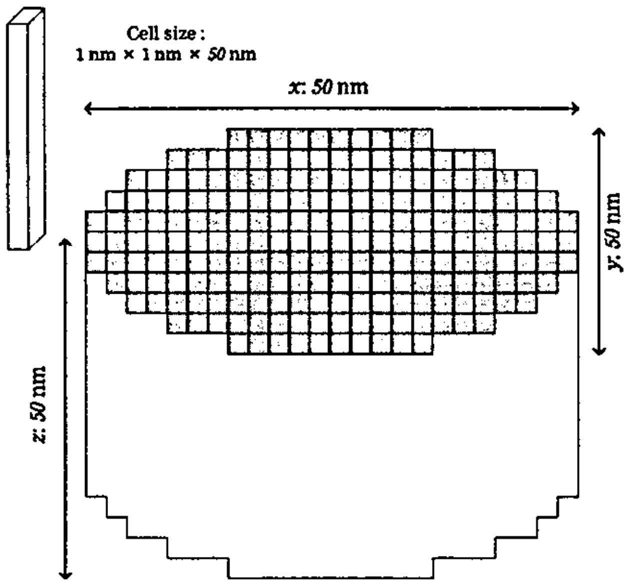

Fig. 5 Core-shell model of a magnetic particle. The shape of the particle is ellipsoid, and the length in each direction is equal.

6.3 表面磁気異方性の顕在による磁気的硬質化

仮想的な鉄系物質 (Table 1) を想定し，その単一磁区微粒子内の磁化の振舞について計算機実験を行った．計算機実験には，米国 NIST が開発し public domain で公開している OOMMF (The Object Oriented Micro-Magnetic Framework), release 1.2 alpha 3 を用いた[32), 33)]．OOMMF は Landau-Lifshits-Gilbert の磁化の動力学式[34), 35)]に基づいて，印加磁場に対し磁気エネルギーが最小となる状態を計算し磁化曲線を求める手法である．

Fig. 5 に示す円柱状試料を仮定し，対象試料を 2 次元格子状のセルに分割し，各格子でスピンを計算する．試料表面において磁気異方性が界面に垂直方向に作用しておりそ

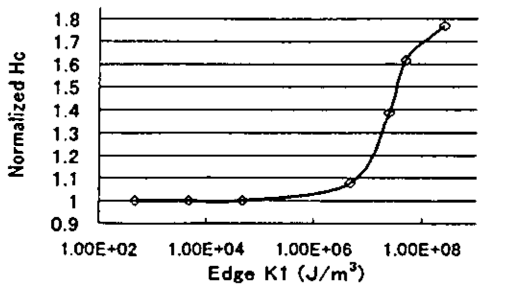

Fig. 6 Calculated coercivity H_c for 50-nm particles with various edge K_1 values. The data are normalized with 195 mT of H_c as obtained when the edge K_1 is equal to K_1.

の異方性定数は，通常のバルクの結晶磁気異方性定数 K_1 とは異なる値（表面磁気異方性定数 edge K_1）をとっているとした．試料サイズ (30, 40, 50 nm) と edge K_1 を変数として実験を行った．この仮定に基づき，外部磁場（X 軸方向）を変化させたときの磁化曲線を求めた結果，edge K_1 が内部の異方性定数に比べて増加するに従って保磁力が漸次に増加（Fig. 6 に一例）し，また単一磁区微粒子でも粒子サイズが小さいほど保磁力が高くなることが明らかとなり，実測のデータ（例えば Fig. 4）と呼応する結果であることが明らかとなった．

Fig. 6 の結果より，単一磁区粒子の保磁力に影響を及ぼすほどの表面磁気異方性の大きさは，バルク体がもつ磁気異方性に比べ桁違いに高い．異方性磁界に換算するとかなり高い値に達する．このことからも表面磁気異方性が付加機能している場合の微粒子を，磁気的に飽和させるためには格段に高い外部磁界が必要であると言える．

7. まとめ

ナノ粒子における特異な構造と磁気的性質について，具体例を提示してその起因などを概説してきた．ナノ粒子の構造と物性を律する要因として，粒子表面層を占める原子数が多いことに端を発するバルク体とは異なる結晶構造の誘発や，イオン性物質ではバルク体とは異なるイオン配置や空格子の出現，温度によるイオンの再配列など，エネルギー的に有利なさまざまな形で特異構造を誘発し，バルク体とは異なる固有の物性を呈していることの一端を紹介したつもりである．ナノ粒子にはそれらに起因する格子歪がさまざまな形で存在し，それがナノ粒子の示すさまざまな特異磁性の根底にある．ナノ粒子の呈する形態・物性はつまるところ，微粒子の全自由エネルギーを最小にする状態として顕在していることになり，その方向に沿う形でナノ粒子はさまざまな自己表現をしていると言える．この拙文が関連分野に携わる方々にいくらかでも参考になれば幸いである．

謝　辞　この小文の骨子は，カナダ国マニトバ大学 A. H. Morrish 教授との長年にわたる共同研究が基になっている．それを補完する実験データは石巻専修大学学部生および院生諸氏の研究成果を中心にまとめたものである．特に，コンピュータシミュレーション実験は本学情報電子工学科助手の川村　暁氏の協力によるものである．関係各位に厚くお礼申し上げたい．一部は厚生労働省科学研究費（課題番号 H14-ナノ-021）の支援を受けて遂行していることを記し謝意を表したい．

文　献

1) K. Haneda: *Canadian J. Phys.*, **65**, 1233 (1987).
2) 羽田紘一: 表面科学, **8**, 427 (1987).
3) 阿部正紀, 松下伸広: 日本応用磁気学会誌, **27**, 721 (2003).
4) S. P. Li, M. Natali, A. Lebib, A. Pépin, Y. Chen, and Y. B. Xu: *J. Magn. Magn. Mat.*, **241**, 447 (2002).
5) R. H. Kodama: *J. Magn. Magn. Mat.*, **200**, 359 (1999).
6) 新井敏弘: 日本応用磁気学会誌, **26**, 51 (2002).
7) A. H. Morrish, K. Haneda , and P. J. Schurer: *J. de Phys.*, **37**, C6-301 (1976).
8) A. H. Morrish and K. Haneda: *J. Magn. Magn. Mat.*, **31–34**, 951 (1983).
9) K. Haneda and A. H. Morrish: *Nucl. Inst. Methods in Phys. Res. B*, **76**, 132 (1993).
10) K. Haneda and A. H. Morrish: *IEEE Trans Magn.*, **35**, 3490 (1999).
11) B. Jeyadevan, K. Shinoda, K. Tohji, and A. Narayanasamy: Ferrites: Proc. Eighth Int. Conf. (ICF8), pp. 790–792, (2000).
12) O. Kitakami, H. Sato, Y. Shimada, F. Sato, and M. Tanaka: *Phys. Rev. B*, **56**, 13849 (1997).
13) T. Majima, K. Haneda, T. Miyahara, T. Itou, T. Ishii, and M. Takami: レーザー科学研究, No. 13, 14 (1991).
14) K. Haneda, Z. X. Zhou, A. H. Morrish, T. Majima, and T. Miyahara: *Phys. Rev. B*, **46**, 13832 (1992).
15) A. H. Morrish and K. Haneda: Ferrites: Proc. Eighth Int. Conf. (ICF8), pp. 247–249 (2000).
16) A. H.Morrish, Z. W. Li, and X. Z. Zhou: *J. Phys. IV, B (France)*, **7**, C1-513(1997).
17) 佐藤寿彦, 羽田紘一, 横山　勝: 材料科学, **31**, 3 (1994).
18) T. Kamiyama, K. Haneda, T. Sato, S. Ikeda, and H. Asano: *Solid State Commun.*, **81**, 563 (1992).
19) K. Haneda and A. H. Morrish: *J. Magn. Soc. Jpn.*, **22** (S1), 255 (1998).
20) P. Novák, J. Englich, H. Stepankova, J. Kohout, H. Lutgemeier, K. Wagner, and W. Tolksdorf: *Phys. Rev. Lett.*, **75**, 545 (1995).
21) K. Wagner, H. Lutgemeier, W. Zinn, P. Novák, J. Englich, H. Dotsch, and S. Sure: *J. Magn. Magn. Mat.*, 140–144, 2107 (1995).
22) P. Novák, J. Englich, H. Stepankova, J. Kohout, H. Lutgemeier, K. Wagner, and W. Tolksdorf: *J. Phys. IV (France)*, **7**, C1-283 (1997).
23) A. H. Morrish, K. Haneda, and X. Z. Zhou: "Surface Magnetism of Nanometer Particles," in Nanophase Materials, ed. by G. C. Hadjipanayis and R. W. Siegel, Kluwer Academic Publishers, pp. 515–535 (1994).
24) J. M. D. Coey and D. Khalafalla: *Phys. Status Solidi A*, **11**, 229 (1972).
25) L. Néel: *J. Phys. et Radium*, **15**, 225 (1954).
26) P. Bruno and J. P. Renard: *Appl. Phys. A*, **49**, 499 (1989).

27) T. Itou, T. Nakajima, K. Doi and K. Haneda: Ferrites: Proc. Eighth Int. Conf. (ICF8), pp. 787–789 (2000).
28) F. Agnoli, Ph. Tailhades, B. Gillot, and A. Rousset: Ferrites: Proc. Eighth Int. Conf. (ICF8), pp. 606–608 (2000).
29) H. Kojima and K. Haneda: *IEEE Trans. Magn.*, **MAG-16**, 11 (1980).
30) N. S. Borrelli, S. L. Chen, and J. A. Murphy: *IEEE Trans Magn.*, 8, 648 (1972).
31) K. Haneda and A. H. Morrish: *Solid State Commun.*, 22, 779 (1977).
32) M. J. Donahue and D. G. Porter: "OOMMF User's Guide, Version 1.0," Interagency Report NISTIR 6376 (1999).
33) M. J. Donahue and R. D. McMichael: *Physica B*, 233, 272 (1997).
34) L. Landau and E. Lifshitz: *Physik. Z. Sowjetunion*, 8, 153 (1935).
35) T. L. Gilbert: *Phys. Rev.*, 100, 1243 (1955).

(2003年7月1日受理)

羽田紘一　はねだ　こういち

昭41　東北大学工学部電子工学科卒，**昭43**　同大学院工学研究科修士課程修了，同年　同学科学計測研究所助手，**昭49～52・54・60・63・平元・8**　カナダ国マニトバ大学併任（博士研究員，客員助教授・同準教授・同教授），**昭63**　東北大学助教授，**平元**　石巻専修大学助教授，**平5**　同学教授，現在に至る．

専門　磁気物性工学，微粒子磁性材料

（工博）

研　　究

強磁性微粒子の保磁力に与える表面磁気異方性の効果－計算 vs. 実測－

川村　暁，羽田　紘一

石巻専修大学理工学部情報電子工学科，〒986-8580 石巻市南境新水戸 1.

Effects of Surface Anisotropy on the Coercivity of Ferromagnetic Small Particles -Computer Simulation vs. Experimental Observations-

Satoshi Kawamura and Koichi Haneda

Department of Information Technology and Electronics, School of Science and Technology, Ishinomaki Senshu University, 1 Sinmito Minamisakai, Ishinomaki 986-8580.

Received May 10, 2004

SYNOPSIS

A computer simulation has been made for a calculation of technical magnetization curves of magnetic small particles in nanometer scale by assuming surface anisotropy acting in addition to existing magneto-crystalline anisotropy in bulk (a particle body). A particle shape modeled is a cylinder, in which a variable particle size of 30, 40, 50 and 60 nm in diameter with a fixed height of 30 nm for each is considered. Micro-magnetic calculations, based on Landau-Lifshitz-Gilbert equation, indicate an enhanced coercivity for a magnetic single-domain particle with the smaller particle size and also with the stronger surface anisotropy acting there, in accord with the existing coercivity data for various materials in small particle forms.

KEY WORDS

surface anisotropy, coercive force, ferromagnetic small particles, micro-magnetic calculation

1　緒　　言

強磁性物質は，同一物質であっても微粒子化することにより多様な磁気特性を得ることができる．それは主として磁化機構および磁化反転機構が，同一物質であっても粒子径によって大きく異なることによるからである．磁性微粒子はこれまで，永久磁石，情報の記録媒体および磁性流体に用いられるなど工業的にも重要な位置を占めてきた[1,2]．また最近では微粒子薄膜として新たな応用を目指す試みや[3]，高密度情報記録を意図した量子化磁気ディスクとして，ナノドット(量子ドット)配列構造の磁気的挙動が注目されている[4]．ナノ構造化にともなう機能性への影響を明らかにし制御につなげることは，この分野の材料設計の観点からも望まれる．

微粒子における特異磁性は，よく知られているようにサイズ効果として磁区構造の変化に起因の技術的磁化に現れるばかりでなく，微粒子という幾何学的構造上の制約を受け物質固有の結晶構造や磁気的性質にも現れる[1,2,5]．ナノ粒子の構造と物性を律する要因は，粒子表面層を占める原子(結合配位数がバルク内原子より減少)数の割合が多いことに端を発すると考えられ，これが起因して格子歪を誘発しナノ粒子はバルク体とは異なる固有の物性を呈することとなる[6]．

今回，磁性微粒子の表面・界面における「表面磁気異方性の誘起」の観点から，マイクロ・マグネティクスの手法を用いて磁性微粒子の磁化過程について計算機シミュレーション実験を行い，種々の磁性微粒子についての実測の磁化特性や高磁場下Mössbauer分光測定データの分析結果(粒子表面層における spin canting 構造の実証)と照合することで有意な結果を得たので報告する．

2　計算機実験の方法

強磁性体粒子はその粒子径を減少させていくと，ある臨界径以下の粒子領域では粒子内に磁区の境界(磁壁)が存在しない方がエネルギー的により安定となり，粒子全域がひとつの磁区から成るいわゆる単一磁区粒子となる．単(一)磁区粒子の磁区内の磁化状態は，巨視的には磁化の向きは一様で磁気異方性エネルギーを最小にするような特定の方向に向いているとされているが，微視的には磁気に関与のエネルギーの総和(交換・異方性・磁歪・静磁エネルギー等)から導かれることとなる．このような単磁区微粒子を計算対象の粒子とした．

計算機実験には，米国NISTが開発しpublic domainで公開しているOOMMF (The Object Micro-Magnetic Framework), release 1.2 alpha 3 [7] を用いた．仮想の鉄系物質を対象とし，その単磁区粒子の磁化の振る舞いについて諸パラメータを設定し磁気履歴曲線を求め，保磁力値について考察を行った．すなわち計算の便宜さおよび計算精度の面からZ軸方向の長さを固定し，X, Y軸方向の長さを可変とした円柱状粒子を対象とし，その円柱比やサイズを変えるとともに，微粒子表面において，通常のバルク体の結晶磁気異方性定数K_1とは異なる起因の磁気異方性が作用しており，その作用方向は任意方向で取り扱い上は問題ないが，計算ではそのうち界面に対しての垂直成分(表面磁気異方性*edge* K_1)の値をパラメータとして，結果に与える影響を調べた．

3 計算過程と結果

計算に用いたOOMMFは，式(1)に示すLandau-Lifshitz-Gilbertの磁化の動力学式[8,9]に基づいて，印加磁場に対し磁気エネルギーが最小となる状態を計算し磁化曲線を求める手法である．

$$\frac{dM}{dt} = -|\bar{\gamma}|M \times H_{eff} - \frac{|\bar{\gamma}|\alpha}{M_s} M \times (M \times H_{eff}) \tag{1}$$

ここで，Mは磁化，H_{eff}は有効磁場，$|\bar{\gamma}|$はLandau-Lifshitz磁気回転比，αはdamping定数，Msは飽和磁化である．

具体的な計算には，Table 1に示すような仮想的な鉄系強磁性物質を想定し，その単一磁区粒子内の磁化の振る舞いについて計算機実験を行った．計算機実験に用いた環境をTable 2に示す．計算対象の粒子として，Fig.1に示す円柱状試料を仮定し，対象試料を2次元格子状のセルに分割し，各セルにおける平均場から各セルでのスピンを計算するという手法により2次元的設定で磁化曲線を求めた．また試料の表面セル層(側面)において，特異な磁気異方性が作用しており，その異方性の界面に対しての垂直成分(Z軸方向)の値をパラメータとして磁化曲線を求めた．試料サイズはZ軸方向を$z=30$ nm一定とし，X軸方向及びY軸方向については$x=y=30, 40, 50, 60$ nmとして実験を行った．それぞれの場合において，*edge* K_1 ($4.8\times10^4 \sim 4.8\times10^7$ J/m^3)を変数とした．

このような設定に基づき，外部磁場(X軸方向)を印加し変化させたときの振る舞いから磁化曲線を求めた(Fig.2)．例として，粒子サイズ40 nmにおいて*edge* K_1の値を変化させたときの磁化曲線のいくつかの例をFig.3に示す．また磁化過程における各セルの磁化状態の一例として，*edge* $K_1=4.8\times10^4$ J/m^{3}の場合における，磁化過程に伴う各セルの磁化状態の変化の

Table 1 The value of material-parameters.

Material-parameters	Value
Saturation magnetization (Ms [A/m])	1.70E+06
Exchange stiffness (A[J/m])	2.10E-11
Crystalline anisotropy constant (K_1[J/m^3])	4.80E4
Surface crystalline anisotropy constant (*edge* K_1[J/m^3])	Variable
Anisotropy type	uniaxial

Table 2 Environment of computer experiment.

Computer	hp Workstation zx2000
CPU	Intel Itanium2 900MHz
Memory	1.5Gbyte
OS	Red Hat Linux Advanced Workstation release 2.1AW
Compiler	gcc 2.96
Software	Object Oriented Micromagnetic Framework (OOMMF) Release 1.2a3

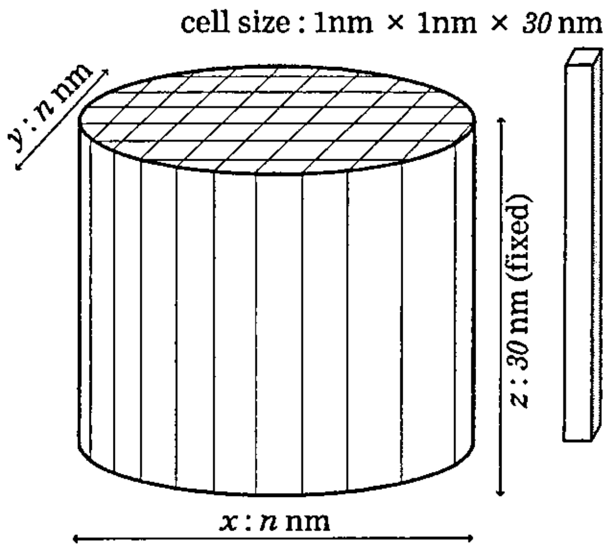

Fig.1 A core-shell model of a magnetic particle. A particle shape is ellipsoid, in which an equilength of x axis and y axis ($x=y=n$, $n=30, 40, 50$ and 60 nm) is assumed for a fixed length of 30 nm for z axis.

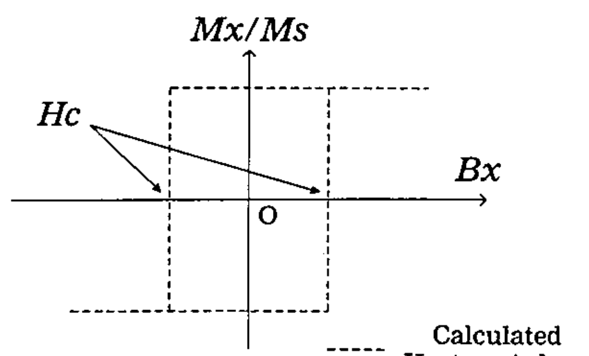

Fig.2 Determination of coercive force (Hc) in a calculated hysteresis loop.

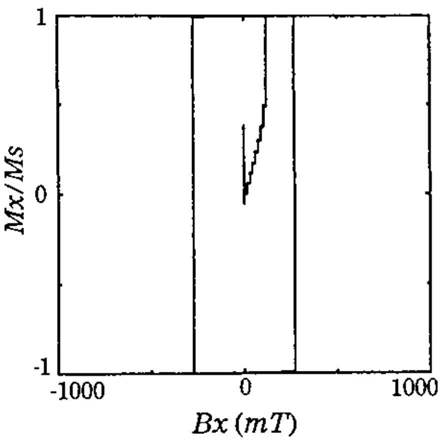

(a)　*Edge* K_I=4.8×10^4
Hc=270 mT.

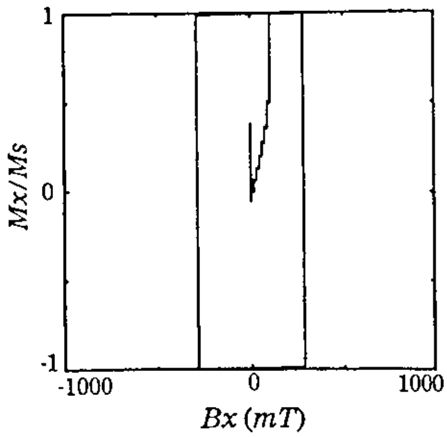

(b)　*Edge* K_I=4.8×10^6
Hc=285 mT.

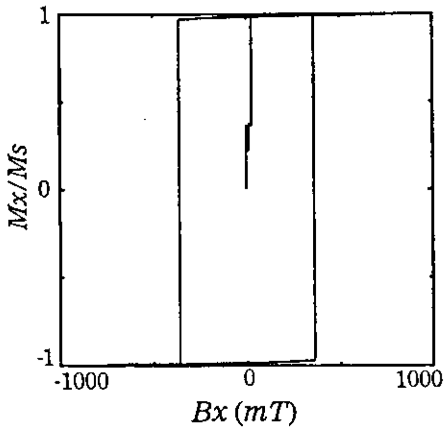

(c) *Edge* K_I= 2.4×10^7
Hc=360 mT.

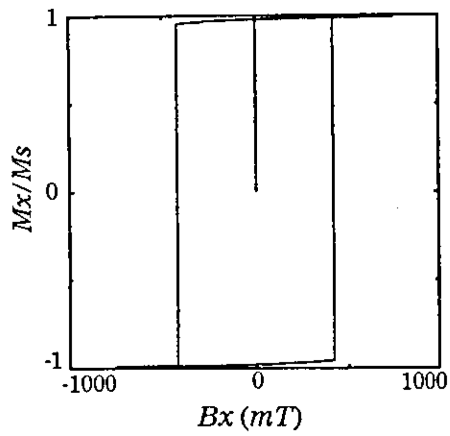

(d) *Edge* K_I= 4.8×10^7
Hc=420 mT.

Fig.3　Examples of technical magnetization curves for 40 nm particles.

様子をFig.4に示す．アトランダムなスピン配列の初期状態(a)からスタートして，まず設定パラメータ下でのマイクロ・マグネティクス的な単磁区粒子の磁化状態(d)に至り，外部磁場の印加に伴う各セルの磁化状態の変化の様子(e),(f)がうかがえる．このようにして色々な粒子サイズについて，*edge* K_Iをパラメータにしての磁化曲線より固有保磁力値を求めた結果をFig.5に示す．*edge* K_Iの値が増加するにしたがって保磁力が漸次に増加し，また単一磁区粒子でも粒子サイズが小さいほど保磁力が高くなる傾向にあることが言える．

4　実測の保磁力値との照合

保磁力に粒子表面層の関与があることを示唆する実験データの一例として，単磁区粒子領域のYIG($Y_3Fe_5O_{12}$)微粒子について4.2 Kでの固有保磁力を比表面積に対してプロットした結果をFig.6に示す[10]．粒子サイズの微細化に伴う比表面積の増加に比例して，固有保磁力値が増加している様相が窺える．粒子サイズが極端に小さな領域で直線性から外れているのは超常磁性的挙動に伴う熱的ゆらぎによるものと思われる．同様の傾向を示すデータは，他の物質(例えばTable 3に示す$NiFe_2O_4$[11]や$Dy_2BiFe_3O_{12}$[12])でも観測されており，磁性微粒子にまつわる特有の性質である．

またFig.5の結果より，単一磁区粒子の保磁力に影響を及ぼすほどの表面磁気異方性の大きさは，バルク体が持つ磁気異方性に比べ桁違いに高く，異方性磁界に換算するとかなり高い値に達する．かような磁性微粒子を，磁気的に飽和させるためには格段に高い外部磁界が必要であるといえる．本節で上に例示した物質はいずれも，高磁場下でのMossbauer分光測定データの分析結果から，粒子表面層におけるspin canting構造(高磁場下でも配向しない磁化)の実在が既に明らかにされており[1]，現象的には計算機実験の結果と相通じるところがある．

微粒子のmagnetic hardeningのメカニズムとしてこれまで着目されてきた要因は，結晶磁気異方性や形状磁気異方性に起因するものが大部分である．これらに加えて表面磁気異方性

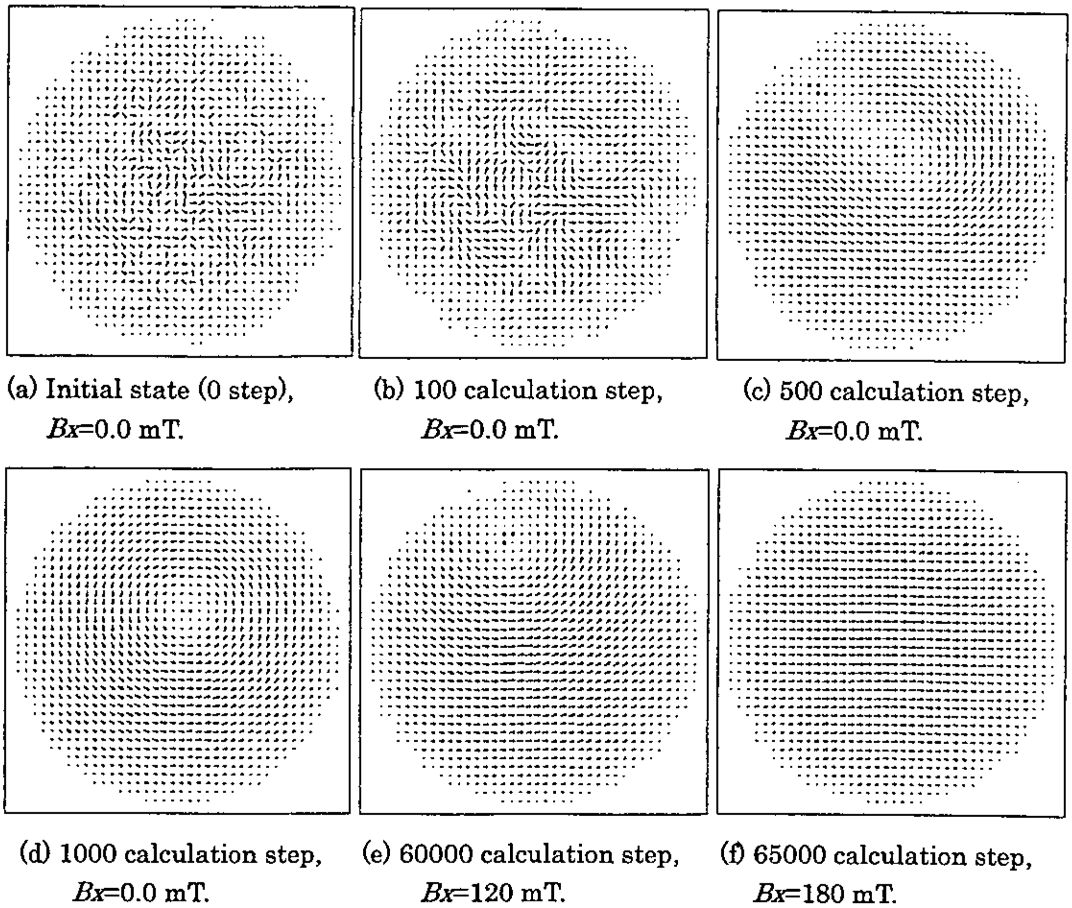

Fig.4 Magnetization state of modeled sample (40 nm particle, *edge* $K_1 = 4.8\times10^4$ J/m^3).

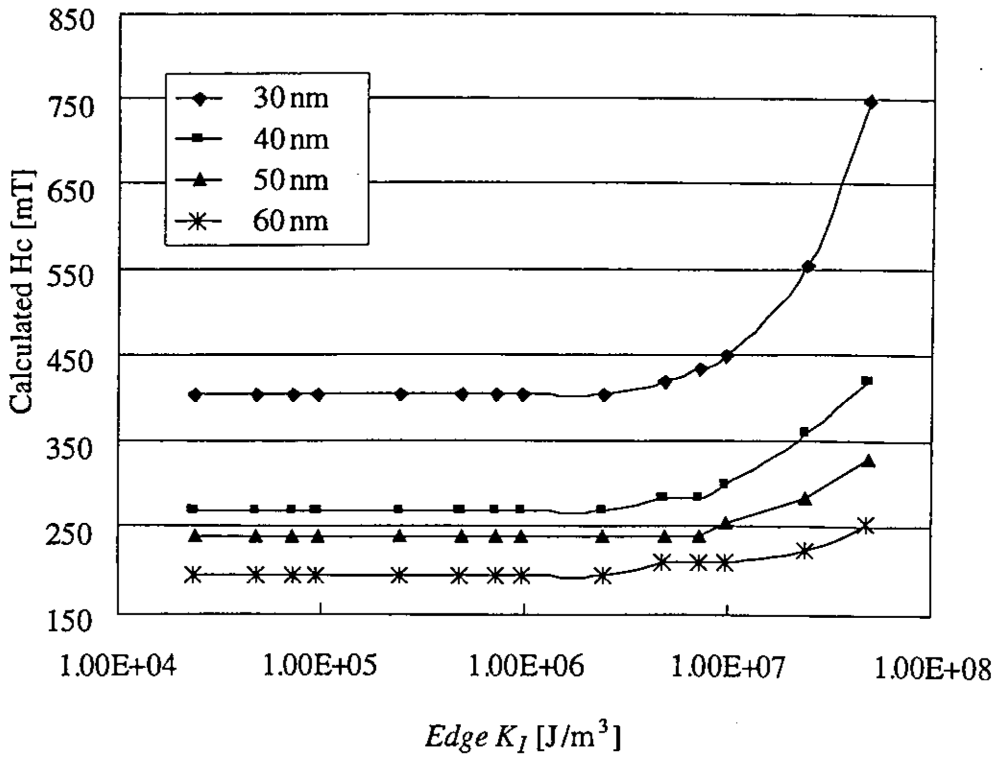

Fig.5 Calculated coercivity *Hc* for various *edge* K_1 parameters for 30 nm, 40 nm, 50 nm and 60 nm particles.

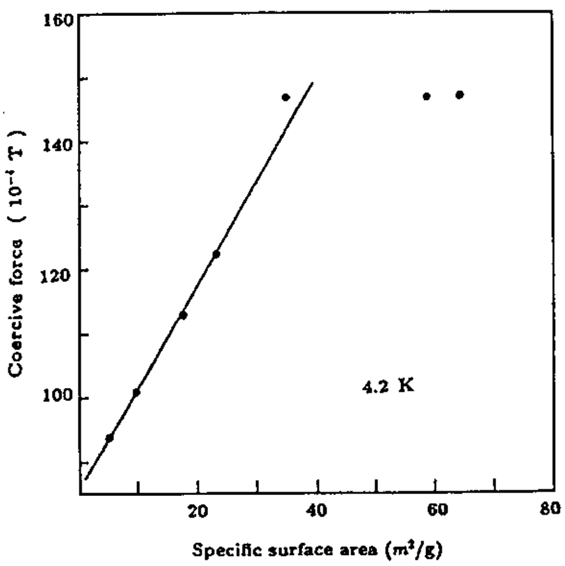

Fig.6 The coercive force of YIG particles with various surface areas at 4.2 K.

が付与された形で更なる磁気的硬質化が期待できるものと考えられる.

5 結 言

ナノ粒子の磁性がバルク体の磁性と異なる所以は，サイズが極度に小さいことによるサイズ効果からの寄与がある点，および粒子表面層の占める割合が大きいことによる表面効果からの寄与があることの2点である．同一物質であっても磁場を作用(磁化過程・減磁過程)させた際の磁気特性の違い，いわゆる技術磁化は，古くから確立されているように大方サイズ効果に起因するものである．これに対し物質定数と考えられてきた自発磁化値(いわゆる固有磁化)は，ナノ化によって大きく変わること(低下する場合が多い)が多くの報告で指摘されており，筆者らのこれまでの研究でそれは粒子表面層において，バルク体とは異なる特異な磁気構造(spin canting構造)が存在することがその原因として確立(表面効果)しつつある．またもう一つの表面効果として，微粒子の特異な表面構造・組織に起因するいわゆる表面磁気異方性の誘起の可能性も示唆されている．

今回，磁性微粒子の表面・界面における「表面磁気異方性の誘起」の観点から，マイクロ・マグネティクスの手法を用いて磁性微粒子の磁化過程について計算機シミュレーション実験を行い，YIG微粒子[13]をはじめ種々の磁性微粒子についての実測の磁化特性データや既報の高磁場下Mössbauer分光測定データの分析結果(粒子表面層におけるspin canting構造の実証)とも呼応する結果が得られた．すなわち計算機実験より固有保磁力値を求めたところ，同一粒子サイズでは*edge* K_1の値が増加するにしたがって保磁力が漸次に増加し，また単一磁区粒子でも粒子サイズが小さいほど保磁力が高くなる傾向にあることが明らかになった．

Table 3 Coercivity data for small $NiFe_2O_4$ particles at 4.2 K.

Particle size (Å)	Crystallite size (Å)	Coercive force (Oe)
250±50	250	600
800±200	400	500
1300±200	500	220

文 献

1) K.Haneda: "Recent advances in the magnetism of fine particles", Canadian J. Phys., 65(1987)1233-1244.
2) K.Haneda: "Magnetic Properties of Ultrafine Particles and Their Applications in Technology", J. Surf. Sci. Soc. Japan (Hyomen Kagaku), 8(1987)427-433.
3) M.Abe and N.Matsushita: "Microwave and Nano-biomagnetic Applications of Ferrite Thin Films and Fine Particles Prepared from an Aqueous Solution", J. Magn. Soc. Jpn., 27(2003)721-729.
4) S.P.Li, M.Natali, A.Lebib, A.Pepin, Y.Chen and Y.B.Xu: "Magnetic nanostructure fabrication by soft lithography and vortex single domain transition Co dots", J. Magn. Magn. Mat., 241(2002)447-452.
5) R.H.Kodama: "Magnetic nanoparticles", J. Magn. Magn. Mat., 200(1999)359-372.
6) K.Haneda: "Structural Distortions in Nanometer particles and Their Magnetic properties", J. Mag. Soc. Japan, 27(2003)993-999.
7) M.J.Donahue and D.J.Porter: "OOMMF User's Guide, Version 1.0", Interagency Report NISTIR 6376, (1999).
8) L.Landau and E.Lifshitz: "On the Theory of the Dispersion of Magnetic Permeability in Ferromagnetic Bodies", Physik. Z. Sowjetunion, 8(1935)153-169.
9) T.L.Gilbert: "A Lagrangian Formulation of the Gyromagnetic Equation of the Magnetization Field", Phys. Rev., 100(1955) 1243.
10) A.H.Morrish, K.Haneda and X.Z.Zhou: "Surface magnetism of nanometer particles", in Nanophase Materials, G.C.Hadjipanayis and R.W.Siegel, eds. Kluwer Academic Publishers, (1994)515-535.
11) A.H.Morrish and K.Haneda: "Magnetic structure of small $NiFe_2O_4$ particles", J. Appl. Phys., 52(1981)2496-2498.
12) K.Haneda and A.H.Morrish: "Magnetic properties of small particles for possible magneto-optical pigments", IEEE Trans. Magn., 35(1999)3490-3495.
13) K.Haneda and A.H.Morrish: "Mössbauer study of Magnetism in YIG Small Particles", J. Magn. Soc. Jpn., 22(S1)(1998)255-257.

Key Engineering Materials Vols. 254-256(2004) pp. 395-398
online at http://www.scientific.net

Consolidation of Multi-Walled Carbon Nanotube and Hydroxyapatite Coating by the Spark Plasma System (SPS)

M. Omori[1], A. Okubo[1], M. Otsubo[2], T. Hashida[2] and K. Tohji[2]

[1] Institute for Materials Research, Tohoku University, 2-1-1 Katahira, Aoba-ku,Sendai 980-8577, Japan, email: mamori@imr.tohoku.ac.jp
[2] Graduate School of Engineering, Tohoku University, Aoba, Aramaki, Aoba-ku, Sendai, 980-8577, Japan

Keywords: carbon nanotube, multi-walled carbon nanotube, consolidation of carbon nanotube, spark plasma system (SPS), spark plasma sintering (SPS), hydroxyapatite coating

Abstract. A multi-walled carbon nanotube (MWNT) was mixed with phenol resin and consolidated by the spark plasma system (SPS). Properties of the MWNT consolidated at 1200°C at 120 MPa were as follows: bulk density was 1.74 g/cm^3; apparent porosity was 16.3%; Young's modulus was 11.1 GPa. Hydroxyapatite was coated on the consolidated MWNT at 1000°C and 120 MPa by SPS, using the suspension prepared from 6 moles of $CaHPO_4 \cdot 2H_2O$ and 4 moles of $Ca(OH)_2$.

Introduction

Carbon nanotubes (CNT) consist of single-walled carbon nantubes (SWNT) and multi-walled carbon nanotubes (MWNT) and have been attracting a lot of attention since their discovery [1]. It is said that molecular circuit devices will be fabricated from SWNT [2]. MWNTs are composed of various kinds of tube diameters and a number of carbon network layers. CNT are still expensive, but the cost of their fabrication will surely decreased in the near future. Low-cost CNTs will be used for fillers of composites and starting materials to produce structural and/or functional compacts. Graphite is a hard-to-sinter material, and its powder can only be sintered at very high temperatures under pressing [3]. The sintering ability of CNT is the same as that of graphite, and advanced techniques are needed to consolidate it at lower temperatures, before the transformation into graphite. The spark plasma system (SPS) has been developed for sintering of metal and ceramics in the plasma and electric field [4, 5], and it is used for consolidation of various kinds of materials such as metals, ceramics and polymers [6]. The bioactivity of graphite is not excellent. The best way to increase the bioactivity of the consolidated MWNT is deposition of hydroxyapatite (HA) films on it. Plasma spraying is widely used for manufacturing HA coating on Ti or Co-Cr-based implants. However, a multitude of phase changes occurs at high temperatures of the plasma spraying process [7]. Two compounds of 6 moles of $CaHPO_4 \cdot 2H_2O$ and 4 moles of $Ca(OH)_2$ reacted at 150°C to produce HA and H_2O by the hydrothermal hot-pressing method [8]. This reaction is able to apply to HA coating on biomaterials because the reaction product is only HA except for H_2O.

In this paper, the MWNT was mixed with phenol resin in ethanol. After removing the ethanol and decomposing the phenol resin by heating, the mixture of the MWNT and the amorphous carbon was consolidated by SPS. The consolidated MWNT was dipped in the suspension of 6 moles of $CaHPO_4 \cdot 2H_2O$ and 4 moles of $Ca(OH)_2$. The two compounds reacted and bonded to the consolidated MWNT at 1000°C at 120 MPa by SPS.

Experimental procedures

Consolidation of MWNT

CNT used for the consolidation was MWNT (NanoLab Inc., USA, 80% purity). The MWNT was purified to remove a metal catalyst using a solution of 50% HNO_3. Phenol resin was dissolved in ethanol. The MWNTs were put in the ethanol solution. After evaporating ethanol, the phenol resin film on the MWNT was decomposed at about 200°C in air. The coated MWNTs were put in a graphite die and set in the spark plasma system (SPS) (Sumitomo Coal Mining, Japan, SPS-1050). The consolidation was carried out between 1000°C and 1600°C at 120 MPa in a vacuum. In case of the consolidation at 1000°C, the consolidation temperature was raised as follows: heating rate from 0°C to 900°C at 100°C/min, from 900°C to 980°C at 20°C/min, from 980°C to 1000°C at 5°C/min and holding time at 1000°C for 5 min.

The microstructure of the consolidated MWNT was analyzed by a transmission electron microscope (JEOL, Japan, JT-007). The polished surface of the consolidated MWNT was observed with an optical microscope (Nikon, Japan, N-01). X-ray diffraction (XRD) was carried out on the MWNT and the consolidated one using Cu Kα line by an X-ray diffractometer (Rigaku, Japan, Rotaflex, RU-200B). Density of the consolidated disk was determined based on Archimedes' principle using water. Elastic modulus of disk samples (3 mm in thickness and 20 mm in diameter) was measured by a pulse-echo overlap ultrasonic technique, using an ultrasonic detector (Hitachi Kenki Co. Ltd., Japan, ATS-100) and a storage oscilloscope (Iwasaki Tsushinki Co. Ltd., Japan, DS6411).

Coating of HA on the consolidated MWNT

$CaHPO_4 \cdot 2H_2O$ (6 moles) and $Ca(OH)_2$ (4 moles) powders (Wako Pure Chemical Ind., Japan, reagent grade) were used to form HA films. These powders were suspended in distilled water using glycolic acid (Wako Pure Chemical Ind., Japan, reagent grade). The consolidated MWNT (1 x 1 x 5 mm^3) was dipped in the suspension and dried. The coated MWNT was put in the graphite die with carbon powders and set in SPS. The coating of HA was carried out at 1000°C at 120 MPa in a vacuum. The heating rate was controlled as follows: from 20°C to 900°C at 100°C/min, from 900°C to 980°C at 20°C/min and from 980°C to 1000°C at 5°C/min. The holding time at 1000°C was 5 min.

Results and discussion

Consolidation of MWNT

An X-ray diffraction pattern of the MWNT was similar to that of graphite (small squares in Fig. 1). As shown in the transmission electron micrograph (TEM) of Fig. 2, the MWNT consisted of varied tube diameters. The dispersion of the diameter was mainly from 10 nm to 50 nm, and a thick MWNT of 200 nm in diameter was found among them.
The MWNT had about 20% amorphous carbon and was not consolidated by SPS. This amorphous carbon did not enhance the consolidation of the MWNT by SPS. A phenol resin was added to achieve the consolidation, and its carbon residue was of about 20%. The optical micrograph revealed that the MWNT consolidated with the 30% phenol resin contained coarse pores. There were no coarse pores in the MWNT consolidated with 50% phenol resin. It was considered that the addition of the 50% phenol resin was adequate to obtain the dense compact. The X-ray diffraction pattern of the MWNT consolidated at 1000°C was similar to those of the MWNT and graphite. When the consolidation was carried out at 1200°C and at 1400°C, the (101) peak was strong compared with other ones. The pattern of the MWNT consolidated at 1400°C was slightly different from that of the MWNT and graphite. The difference was emphasized on the pattern of the MWNT consolidated at 1600°C, but the intensity of the (101) peak decreased, as shown in Fig. 1. The new diffraction peaks did not correspond to those of graphite. Fig. 3 shows the TEM image of the MWNT consolidated at 1600°C with 30% phenol resin. The MWNT was partly decomposed and converted into different

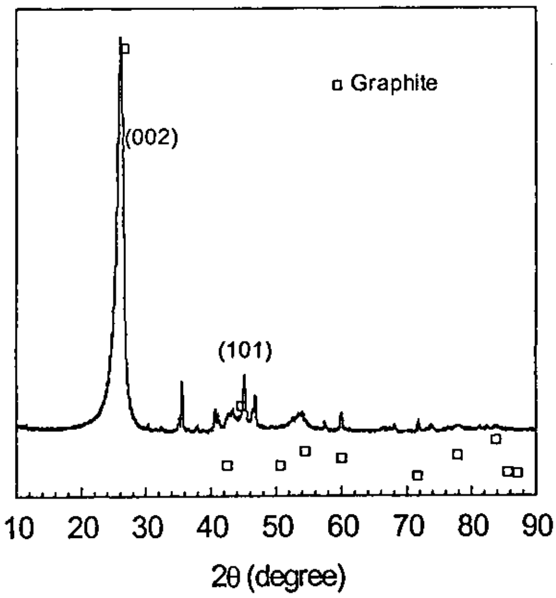

Fig. 1 XRD pattern of the MWNT consolidated at 1600 °C.

Table 1 Density and mechanical properties of the consolidated MWNT

Consolidation temperature (°C)	Bulk density (g/cm^3)	Apparent porosity (%)	Closed porosity (%)	Young's modulus (GPa)	Poisson's ratio
1000	1.67	16.7	9.6	3.05	- 0.62
1200	1.74	16.8	6.4	11.1	0.074
1400	1.73	15.6	8.1	10.1	0.034

compounds from graphite. MWNT is not decomposed until 2400°C by heating [9]. The SPS process consists of some effects such as the spark plasma, electric field and others, and carbon fibers are decomposed into powders by the SPS treatment [6]. The carbon network of the MWNT should be partly decomposed by the spark plasma and resulted in new structures different from graphite.

The density and mechanical properties are shown in Table 1. The low bulk density of the MWNT consolidated at 1000°C indicated that the consolidation was not accomplished. The bulk density of 1.74 g/cm^3 was not high and depended on the tube structure because there were no coarse pores. The apparent porosity was almost the same for all consolidated MWNT. The closed porosity was calculated from the apparent porosity and theoretical density of graphite (2.266 g/cm^3). Since the theoretical density of the MWNT must be lower than that of graphite, the closed porosity should decrease less than the values indicated in Table 1. Young's modulus and Poisson's ratio were measured on the surface where the MWNT was aligned parallel to the pressing direction of SPS. Young's modulus of the MWNT consolidated at 1000°C was lower than that of the ones consolidated 1200°C and 1400°C. The Young's modulus of 11.1 GPa of the consolidated MWNT was not low, considering the density of the consolidated MWNT and that of 16 GPa of a commercial graphite product with high density of 2.0 g/cm^3. Given that, the Young's modulus of human bone is 7 - 30 GPa [9], the consolidation of the MWNT could produce the material with the low modulus. Poisson's ration was negative for the MWNT consolidated at 1000°C, and was very little for the ones consolidated at 1200°C and 1400°C. The negative Poisson's ratio indicated that the bond between the MWNTs was not completed at 1000°C, which is consistent with the Young's modulus of 3.05 GPa.

The bending strength of the consolidated MWNT was measured by a three-point bending test method, but it was not obtained. The sample for the bending test was curved by stress at first, and then it was fractured. Bending strength of ductile materials like metals cannot be measured. The consolidated MWNT behaved in the same way as metal for bending test. Bending strength of human bone is 50 – 150 MPa [9], and that of the consolidated MWNT seemed to be lower than it. It is obvious the strength of the consolidated MWNT is not enough for application to human bone at the moment.

Fig. 2 TEM image of MWNT.

Fig. 3 TEM image of the MWNT consolidated at 1600 °C.

Coating of HA on the consolidated MWNT

$CaHPO_4 \cdot 2H_2O$ and $Ca(OH)_2$ were easily suspended in water compared with HA powder because they contained an OH group or H_2O. The mirror surface of the consolidated MWNT was inadequate for HA coating. A coarse surface was prepared by polishing with SiC powders of 64 □m. Two suspended compounds of 6 moles of $CaHPO_4 \cdot 2H_2O$ and 4 moles of $Ca(OH)_2$ were coated on the consolidated MWNT and reacted at 1000°C and 120 MPa by SPS. The reacted film was identified as HA by X-ray diffractometry. Fig. 4 shows an optical micrograph of the consolidated MWNT coated with HA. The HA film did not contain cracks. The coated HA seemed bonded with the rough surface of the consolidated MWNT, although the bonding strength was not determined. The bonding was partly based on the anchor effect of the coarse surface. It was not clear whether the chemical bond was associated with the bonding. The compounds of 6 moles of $CaHPO_4 \cdot 2H_2O$ and 4 moles of $Ca(OH)_2$ were allowed to dehydrate and produce HA at high pressure, such as 120 MPa. HA was not formed at 1000°C and 10 MPa from those compounds by SPS. The reaction temperature decreased from 1000°C to 600°C with increasing the pressure from 120 MPa to 300 MPa [13], but the film coated at the low temperature peeled. HA can be formed from $CaHPO_4$ or $CaHPO4 \cdot 2H_2O$ at 200°C by hydrothermal technique [10-12]. The reaction temperature by SPS was higher than those of hydrothermal and hydrothermal hot-pressing methods. The hydrothermal reaction requires water to complete the formation of HA, but SPS does not.

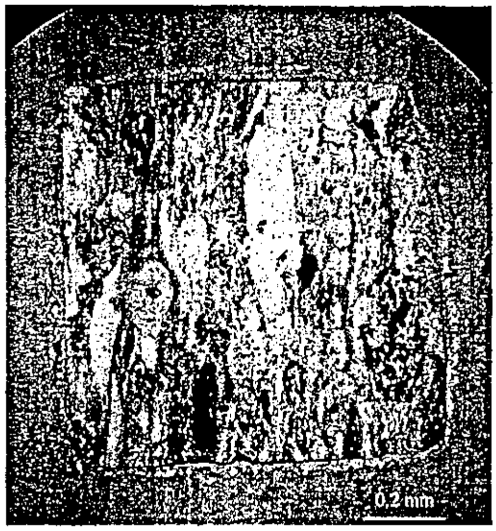

Fig. 4 Optical micrograph of the consolidated MWNT coated with HA.

Conclusions
The MWNT containing about 20% of amorphous carbon was not consolidated by SPS. Amorphous carbon transformed from the phenol resin enhanced the consolidation. The structure of the consolidated MWNT was almost the same as that of graphite. The MWNT in the consolidated form was aligned in the direction parallel to the (101) plane of graphite. The consolidated MWNT was decomposed at temperatures higher than 1400°C. Properties of the MWNT consolidated at 1200°C and 120 MPa were as follows: density was 1.74 g/cm3; apparent porosity was 16.8%; Young's modulus was 11.1 GPa; Poisson's ratio was 0.074.
HA was coated on the consolidated MWNT at 1000°C at 120 MPa, using the suspension prepared from 6 moles of $CaHPO_4 \cdot 2H_2O$ and 4 moles of $Ca(OH)_2$. HA was not cracked and tightly covered the surface of the consolidated MWNT.

Acknowledgments
This study is supported by Research on Advanced Medical Technology in Health and Labour Sciences Research Grants from Ministry of Health, Labour and Welfare of Japan. The authors are thankful to Yoshihiro Murakami, Shun Ito, Yuichiro Hayasaka and Yoshiyuki Sato for the measurements of X-ray diffraction patterns and observations of transmission electron microscope and optical microscope.

References
[1] S. Iijima: Nature, Vol. 354 (1991), p. 56.
[2] L. Chico, L. X. Menedic, S. G. Louie and M. L. Cohen: Phys. Rev., B54 (1996), p. 2600.
[3] H. Boeder and E. Fitzer: Carbon, Vol. 8 (1970), p. 453.
[4] K. Inoue: US Patent, No. 3,241,956 (1966).
[5] K. Inoue: US Patent, No. 3,250,892.
[6] M. Omori: Mater. Sci. Eng., A287 (2000), p. 183.
[7] S. R. Radin and P. Ducheyne: J. Mater. Sci.: Mater. Med. Vol. 3 (1992), p. 33.
[8] K. Hosoi, T. Hashida, H. Takahashi, N. Yamazaki and T. Korenaga: J. Am. Ceram. Soc., Vol. 79 (1996), p. 2771.
[9] A. Bougrine, N. Dupont-Pavlovsky, A Naji, J. Ghanbaja, J. F. Mareche and D. Billaud: Carbon, Vol. 39 (2001), p.685.
[10] L. H. Hench: J. Am. Ceram. Soc., Vol. 81 (1998), p. 1705.
[11] A. P. Peroff and A. S. Posner: Science, Vol. 124 (1958),p. 583.
[12] E. Hayek, W. Boehler, J. Lechleitner and H. Petter: Z. Anorg. Allge. Chem., Vol. 295 (1958), p. 241.
[13] M. Omori, T. Onoki and T. Hashida: Unpublished data

研　　究

Preparation of Multi-Walled Carbon Nanotube Compact by the Spark Plasma System (SPS)

Mamoru Omori[*1], Akira Okubo[*2], Toshiyuki Hashida[*1] and Kazuyuki Tohji[*1]

[*1]Graduate School of Engineering, Tohoku University, 6-6-01 Aoba, Aramaki, Aoba-ku, Sendai 980-8579.
[*2]Institute for Materials Research, Tohoku University, 2-1-1 Katahira, Aoba-ku, Sendai 980-8577.

Received September 30, 2004

SYNOPSIS

The multi-walled carbon nanotube (MWNT) was not consolidated without additives by the spark plasma system (SPS). The phenol resin of 33 wt% was added to promote the consolidation. The MWNTs were aligned perpendicular to pressing direction of SPS in the consolidated compact. Bulk density and Young's modulus were more than 1.7 g/cm^3 and 10 GPa for the MWNT consolidated at 120 MPa at 1200°C and 1400°C. The fracture behavior on bending test was a kind of quasiplastic deformation and was based on pull out of the MWNTs.

KEY WORDS

Carbon nanotube, multi-walled carbon nanotube, consolidation of multi-walled carbon nanotube, multi-walled carbon nanotube compact

1 Introduction

Carbon nanotubes (CNTs), which were discovered in 1991[1], are long, slender fullerenes where the walls of the tubes are hexagonal carbon (graphene layer) and often caped at each end. A lot of investigations have been shown that CNTs exhibit many superior mechanical, electric and electronic properties over any other known material and hold substantial promise as high-strength composites, energy storage and energy conversion devices, sensors, field emission displays and radiation sources, hydrogen storage media and nanometer-sized semiconductor devices[2]. CNT consists of single-walled carbon nanotube (SWNT)[3,4], double-walled carbon nanotube (DWNT)[5] and multi-walled carbon nanotube (MWNT)[1]. One of interests arises from their formidable mechanical properties, i.e. Young's modulus up to 640 GPa for SWNT[6] and up to 1800 GPa for MWNT[7] and strength up to 45 GPa for SWNT[8]. CNT is expensive these days, but the cost of its fabrication will surely decrease in near future. Low-cost CNTs will be useful for fillers of composites and starting materials to produce structural and/or functional compacts. Graphite is a hard-to-sinter material, and its powder can only be sintered at very high temperatures under pressing[9]. The sintering ability of CNT is the same as that of graphite, and advanced techniques are needed to consolidate it at lower temperatures before transforming into graphite. The spark plasma system (SPS) has been developed for sintering of metal and ceramics in the plasma and electric field[10], and it has been used for consolidation of various kinds of materials such as metals, ceramics and polymers[11].

In this paper, the MWNT was mixed with phenol resin in ethanol. After removing the ethanol and decomposing the phenol resin by heating, the mixture of the MWNT and the amorphous carbon transformed from the phenol resin was consolidated by SPS. Bulk density, Young's modulus, and Poisson's ratio were determined for the consolidated MWNT.

2 Experimental Procedures

CNT used for the consolidation was MWNT (NanoLab Inc., USA). Purity of the MWNT is more than 80%, and most of impurities are amorphous carbon. The MWNT was purified to remove metal catalysts by using 50% HNO_3 solution. The novolak type of phenol resin was dissolved in ethanol. The MWNTs were put in the ethanol solution. After evaporating ethanol, the phenol resin film on the MWNT was decomposed at about 200°C in air. The coated MWNTs were put in a graphite die and set in the spark plasma system (SPS) (Sumitomo Coal Mining Co. Ltd., SPS-1050). The consolidation was carried out between 1000°C and 1600°C at 120 MPa in a vacuum. In case of the consolidation at 1000°C, the consolidation temperature was raised as follows: heating rate from 0°C to 900°C at 100°C/min, from 900°C to 980°C at 20°C/min, from 980°C to 1000°C at 5°C/min and holding time at 1000°C for 5 min.

The microstructure of the consolidated MWNT was analyzed by a transmission electron microscope (JEOL, JT-007). The polished surface of the consolidated MWNT was observed with an optical microscope (Nikon, N-01). X-ray diffraction (XRD) was carried out on the MWNT and the consolidated one using Cu Kα line by an X-ray diffractometer (Rigaku, Rotaflex, RU-200B). Density of the consolidated disk was determined based on Archimedes' principle using water. Elastic modulus of disk samples (3 mm in thickness and 20 mm in diameter) was measured by a pulse-echo overlap ultrasonic technique, using an ultrasonic detector (Hitachi Kenki Co. Ltd., ATS-100) and a storage oscilloscope (Iwasaki Tsushinki Co. Ltd., DS6411).

3 Results and Discussion

The TEM image of the MWNT is shown in Fig. 1. The major part of tube diameters was 20−40 nm, and the biggest one rarely observed in the TEM photograph was about 200 nm. Amorphous carbon was identified by TEM and estimated less than 20 %.

The MWNTs consisting of amorphous carbon were not consolidated by SPS, which was not activated by SPS and did not play a roll to combine each MWNT. The phenol resin was added to achieve the consolidation, and its carbon residue was of about 20%. The optical micrograph revealed that the MWNT consolidated with the 23% phenol resin contained coarse pores, as shown in Fig. 2. Much of the phenol resin promoted to get ride of the pores, and coarse pore was not produced in the MWNT consolidated with 33% phenol resin. Fig. 3 shows that there was no coarse pore on the polished surface of the consolidated MWNT. Block patterns were observed in these photographs and indicated a structural regularity. The MWNTs were very roughly aligned in the block, and direction of the alignment was different in each one. The reason why the MWNT was ordered by SPS was not clear, but the ordered alignment might be due to the weak interaction between MWNTs, SWNT forming the bundle structure by strong interaction.

TEM image of the MWNT consolidated at 1400°C is shown in Fig. 4. The MWNTs were aligned in the plane perpendicular to the pressing direction of SPS. The same alignment was observed for the MWNT consolidated at 1000°C and 1200°C. The alignment was not random in

Fig.1 TEM image of MWNT.

Fig.2 Optical micrograph of the MWNT consolidated with 23 wt% of phenol resin at 1000°C at 120 MPa for 5 min.

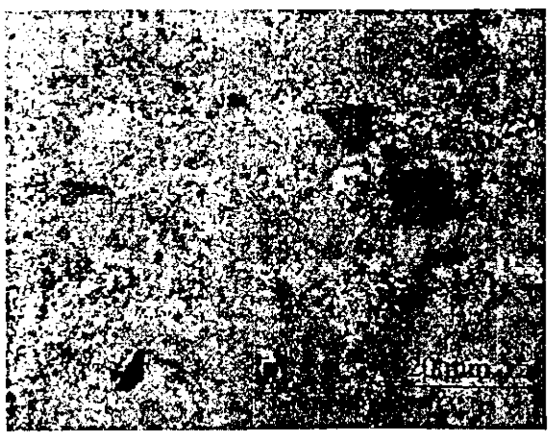

Fig.3 Optical micrograph of the MWNT consolidated with 33 wt% of phenol resin consolidated at 1200°C at 120 MPa for 5 min.

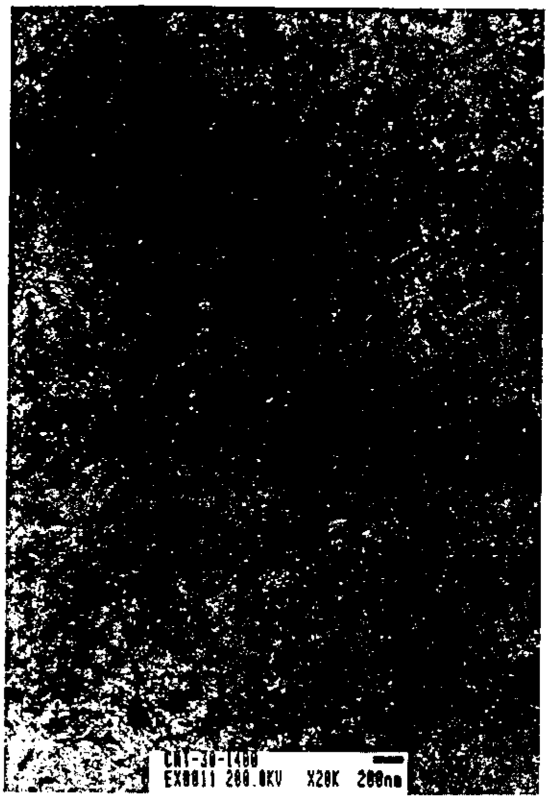

Fig.4 TEM image of the MWNT consolidated at 1400°C at 120 MPa for 5 min.

Fig.5 TEM image of the MWNT consolidated at 1600°C at 120 MPa for 5 min.

this plane, and some regularity was found in it. The MWNTs tended to be in line each other in the small area. When the regularity expanded to the large area, the block pattern may be formed. The diameter of the consolidated MWNT was more than 100 nm and larger than that of the starting MWNT. This growth did not occur during the consolidation but was caused during the ion thinning process for TEM, where argon plasma being used. The structure of the MWNT was partially decomposed at 1600°C by SPS, and graphite-like materials were formed, as shown in Fig. 5. However, the tube structure persisted in this consolidated MWNT.

Fig. 6 shows X-ray diffraction patterns of the MWNT consolidated with the phenol resin of 33% at 1000°C–1600°C at 120 MPa. The diffraction pattern of the MWNT was measured at the same time. Diffraction angle and intensity of graphite were pointed by open circle in Fig. 6. The diffraction pattern of MWNT was different from that of graphite, as shown in Fig. 6a. Several diffraction peaks not assigned to graphite were at about $2\theta=38°$ and between $2\theta=42°$ and $2\theta=47°$, and all of them was based on the tube structure. The diffraction pattern of the MWNT consolidated at 1000°C, which is shown in Fig. 6b, was

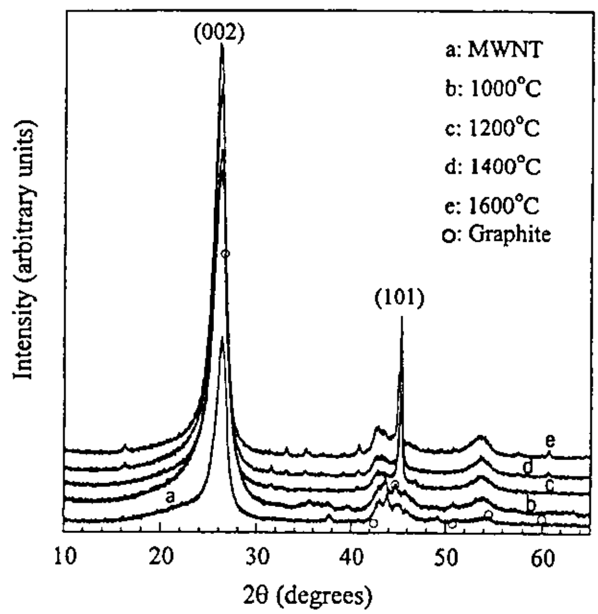

Fig.6 X-ray diffraction pattern of MWNT and the consolidated one.

slightly different from that of the MWNT. The difference was that a small peak appeared near $2\theta=36°$, and it was not found in the diffraction pattern of graphite. When the consolidation temperature was raised higher than 1200°C, the (101) peak of graphite was strong compared with others. X-ray diffraction patterns of the MWNT consolidated at 1200°C, 1400°C and 1600°C are shown in Figs. 6c, 6d and 6e, respectively. The X-ray diffraction was measured on the plane perpendicular to the pressing direction, and the MWNTs were parallel aligned in it. It was revealed that the tube of the MWNT was made of rolled-up sheets of the (101) plane. The (101) peak was not clear on the MWNTs which were not consolidated. On the other hand, the MWNTs were closely connected in the dense MWNT, and X-ray diffracted through the several MWNTs. The difference from graphite was emphasized on the diffraction pattern of the MWNT consolidated at 1400°C, as shown in Fig. 6e. New diffraction peaks, which were not assigned to graphite, appeared between $2\theta=30°$ and $2\theta=42°$. It is obvious that decomposition of the MWNT started at 1400°C. The intensity of new peaks became strong for the MWNT consolidated at 1600°C, and the decomposition progressed further. The MWNT was converted into different compounds from graphite. MWNT is not decomposed until 2400°C by heating[12]. The SPS process consists of some effects such as the spark plasma, electric field and others, and carbon fibers are sectioned into powders by the SPS treatment[9]. Graphen layer of the MWNT was decomposed by the spark plasma and resulted in structures different from graphite.

The bulk density and mechanical properties are shown in Table 1. The low bulk density of the MWNT consolidated at 1000°C indicated that the consolidation was not accomplished. The bulk density of 1.74 g/cm^3 was not high and depended on the tube structure because there was no coarse pore. The apparent porosity was almost the same for all consolidated MWNT. The closed porosity was calculated from the apparent porosity and theoretical density of graphite (2.266 g/cm^3). Since the theoretical density of the MWNT must be lower than that of graphite, the closed porosity should decrease less than the values indicated in Table 1. Young's modulus and Poisson's ratio were measured on the surface where the MWNT was aligned parallel to the pressing direction of SPS. Young's modulus of the MWNT consolidated at 1000°C was less than that of the ones consolidated 1200°C and 1400°C. The Young's modulus of 11.1 GPa of the consolidated MWNT was not little, considering 16 GPa of a commercial graphite product with high density of 2.0 g/cm^3. Poisson's ratio was negative for the MWNT consolidated at 1000°C, and was very little for the one consolidated at 1200°C and 1400°C. The negative Poisson's ratio explained that the bond between the MWNTs was not completed at 1000°C, which is consistent with the Young's modulus of 3.05 GPa. The little Poisson's ratio was explainable that the MWNTs were not tightly connected each other by the amorphous carbon, which being converted from the phenol resin and did not result in strong graphite at 1000°C−1600°C.

Table 1 Bulk density and properties of the MWNT consolidated at 120 MPa for 5 min.

Consolidation temperature (°C)	Bulk density (g/cm^3)	Apparent porosity (%)	Closed porosity (%)	Young's modulus (GPa)	Poisson's ratio
1000	1.67	16.7	9.6	3.05	-0.62
1200	1.74	16.8	6.4	11.1	0.074
1400	1.73	15.6	8.1	10.1	0.034

Bending strength of the consolidated MWNT was measured by a three-point bending test method but was not obtained. The sample for the bending test was curved by stress at first, and then it was fractured. This behavior was a kind of quasiplastic deformation. The consolidated MWNT behaved in the same way as plastic deformation of metal.

SEM image of the fractured surface of the MWNT consolidated at 1000°C is shown in Fig. 7. Most diameter of the MWNTs was not larger than 20−40 nm, and the growth of them did not occur during the SPS consolidation. The majority of the MWNTs were pulled out, and it was hard to find cross sections of the MWNTs which were

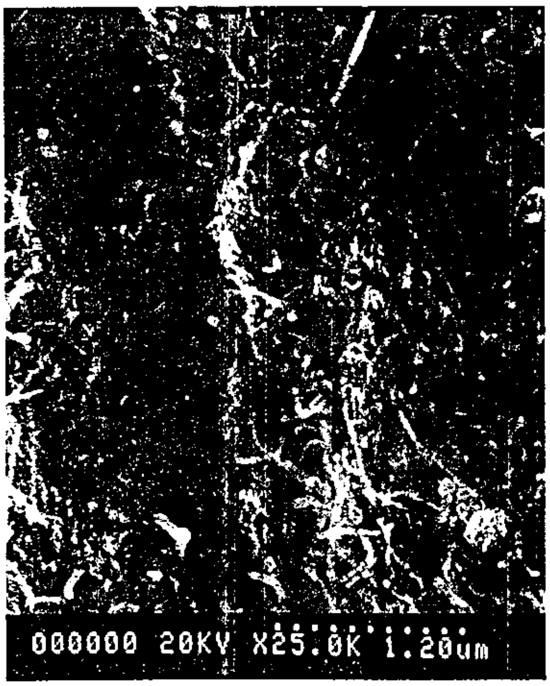

Fig.7 SEM image of the MWNT consolidated at 1000°C at 120 MPa for 5 min.

Fig.8 SEM image of the MWNT consolidated at 1200 °C at 120 MPa for 5 min.

ruptured during the bending test. The consolidation at 1200 °C resulted in a different fractured pattern. The fractured smooth surface and cross section were observed in Fig. 8. The MWNTs were connected more tightly at 1200 °C than at 1000 °C, and some of them were cut. The similar SEM image was given by the MWNT consolidated at 1400 °C. There were a lot of pulled-out MWNTs in these two fractured surfaces, because the bonding amorphous carbon was weak compared with the MWNT. The pull out phenomenon corresponded to the quasiplastic deformation on the three point bending test.

4 Summary

The MWNT was consolidated with the amorphous carbon converted from the phenol resin by SPS. The consolidated MWNTs were aligned in the plane perpendicular to the press direction of SPS in the consolidated compact. The alignment was not random in the plane, but the MWNTs tended to be in line in small area. The tube was rolled up with the (101) plane of graphite, being conformed by X-ray diffraction pattern of the consolidated MWNT. Bulk density and Young's modulus were more than 1.74 g/cm^3 and 11.1 GPa for the MWNT consolidated at 1200 °C at 120 MPa. The fracture behavior on the bending test was a kind of quasiplastic deformation and based on pull out of the MWNTs.

Acknowledgment

This study is supported by Research on Advanced Medical Technology in Health and Labour Sciences Research Grants from Ministry of Health, Labour and Welfare of Japan. The authors are thankful to Yoshihiro Murakami, Shun Ito, Yuichiro Hayasaka and Yoshiyuki Sato for the measurements of X-ray diffraction patterns and observations of transmission electron microscope and optical microscope.

References

1) S.Iijima: "Helical Microtubules of Graphitic Carbon", Nature, 354(1991)56-58
2) R.H.Baughman, A.A.Zakhidov and W.A.de Heer: "Carbon Nanotube - the Route Toward Applications", Science, 297(2002)787-792.
3) S.Iijima and T.Ichihashi: "Single-Shell Carbon Nanotubes of 1-nm Diameter", Nature, 363(1993)603-605.
4) D.S.Bethune, C.H.Kiang, M.S.Devries, G.Gorman, R.Savoy, J.Vazquez and R.Beyers: "Cobalt-Catalyzed Growth of Carbon Nanotubes with Single-Atomic-Layer Walls", Nature, 363(1993)605-607.
5) J.C.Charlier and J.P.Michenaud: "Energetics of Multilayered Carbon Tubules", Phy. Rev. Lett., 70[17](1993)1858-1861.
6) G.Gao, T.Çağin and W.A.Goddard III: "Energetics, Structure, Mechnical and Vibrational Properties of Single-Walled Carbon Nanotubes", Nanotechnology, 9(1998)184-191.
7) M.M.J.Treacy and T.W.Ebbesen: "Exceptionally High Young's Modulus Observed for Individual Carbon Nanobtubes", Nature, 381(1996)678-680.
8) D.A.Walters, L.M.Ericson, M.J.Casavant, J.Liu, D.T.Colbert, K.A.Smith and R.E.Smalley: "Elastic Strain of Freely Suspended Single-Wall Carbon Nanotube Ropes", Appl. Phy. Lett., 74[25](1999)3803-3805.
9) H.Böder and E.Fitzer: "Effect of Hot-Pressing on the Structure of Carbon Artifacts", Carbon, 8(1970)453-454.
10) K.Inoue: US Patent, No. 3,241,956(1966).
11) M.Omori: "Sintering, Consolidation, Reaction and Crystal Growth by the Spark Plasma System (SPS)", Mater. Sci. Eng., A287(2000)183-188.
12) A.Bougrine, N.Dupont-Pavlovsky, A.Naji, J.Ghanbaja, J.F.Marêché and D.Billaud: "Influence of High Temperature Treatments on Single-Walled Carbon Nanotubes Structure, Morphology and Surface Properties", Carbon, 39(2001)685-695.

Bonding property of Hydroxyapatite and Titanium Treated with Hydrothermal Alkali Solution

T. Onoki*, K. Hosoi** and T. Hashida*
*Fracture Research Institute, Graduate School of Engineering, Tohoku University
01 Aoba, Aramaki, Aoba-ku, Sendai, 980-8579, JAPAN
**Shiraishi Kogyo Kaisha Limited
4-78 Motohama-cho, Amagasaki, 660-0085, JAPAN

Introduction

Titanium (Ti) and its alloy are widely used as orthopedic and dental implant materials because of their high mechanical strength, low modulus and good corrosion resistance [1]. However, when embedded in the body, a fibrous tissue capsules the implant isolating from the surrounding bone forms.

Some bioactive ceramics such as hydroxyapatite, bioglass and glass ceramics can directly bond to living bone when used as bone replacement materials [2]. Hydroxyapatite ceramics with formula $Ca_{10}(PO_4)_6(OH)_2$ (HAp) are biomaterials which have been extensively developed recently [3]. In the preparation procedures employed to date, HAp powder was molded first, and then sintered at high temperatures over 1,300°C [4]. The mechanical properties of bulk HAp only allow applications for small non-loaded structure. The possibility of depositing it into films has permitted to exploit its bioactive properties in structural prostheses such as for teeth root, hip, knee and shoulder joint replacement. Therefore, HAp is used as coating materials of those prostheses surface in order to prepare bioactive layers on titanium and its alloys. The HAp surface improves the fixation of implants by the growth of bone into the coating, forming a mechanical interlock.

Plasma spraying techniques have traditionally been used in process of hydroxyapatite coating[5]. However, this high temperature method results in a number of significant problems, including phase and chemical decomposition of the HAp, absence of a chemical interface/bond between the HAp coating and substrate.

We have recently reported a new HHP method for bonding HAp ceramics and Titanium [6]. The hydrothermal reaction of calcium hydrogen phosphate dihydrate ($CaHPO_4 \cdot 2H_2O$; DCPD) and calcium hydroxide ($Ca(OH)_2$) occurs in a liquid phase as follows:

$$6CaHPO_4 \cdot 2H_2O + 4Ca(OH)_2 \rightarrow Ca_{10}(PO_4)_6(OH)_2 + 18H_2O \quad (1)$$

It is known that the water of crystallization in DCPD is slowly lost below 100 °C. If the released water can be utilized as a reaction solvent during the HHP treatment, it is to be expected that the synthesis of HAp, the solidification of HAp and the joining HAp to metal can be achieved simultaneously under the hydrothermal condition.

Recently, it was reported that Ti surface treated with NaOH solution had the ability of joining to HAp directly by a biomimetic method [7].This report describes the effects of alkali solution treatment to Ti on the HAp/Ti interface properties produced by hydrothermal hot-pressing (HHP) method.

Experimental

Firstly DCPD used as a starting powder was prepared by mixing 1.0*M* calcium nitrate solution ($Ca(NO)_3 \cdot 4H_2O$; KANTO CHEMICAL CO., INC., 99.0%) and 1.0*M* diammonium hydrogen phosphate solution ($(NH_4)_2HPO_4$; KANTO CHEMICAL CO., INC., 98.5%). The mixing was carried out at *a* room temperature (approximately 20°C). The precipitate from the mixture was filtered and washed with deionized water and acetone. The washed filter cake was oven-dried and then ground to a powder.

A commercially available pure Ti rod, 20mm in diameter, was used as a bioinert material. The Ti rod was cut into disks with a thickness of 10mm. And the disks were cleaned in deionized water and acetone by using ultrasonic cleaner. Ti surfaces were treated with alkali solution(5*M* NaOH). The conditions of alkali solution treatment were shown in Table1. The conditions of A and B were respectively the same conditions in reference [7]. The condition of A was Ti disks immersed in NaOH solution for 24h. The condition of B was Ti disks were put the heating 600°C after the immersion additionally. The condition of C was utilized the solvo-thermal reaction of NaOH. After these NaOH solution treatments, the Ti disks were washed by deionized water, and then dried in air. In order to characterize the titanium surfaces, the surfaces were observed using scanning electron microscopy (Hitachi FE-SEM S-4300) and examined using FT-Raman spectroscopy. The microprobe instrument used for the FT-Raman spectroscopy consisting of a JOBIN YVON-SPEX spectrometer fitted with a microscope (OLYMPUS-BX40) which allows a spatial resolution on the sample close to 1μm. The 632.8nm line of an He-Ne laser was used as excitation, focused in a spot of